Draft version May 25, 2001
Preprint typeset using LaTeX style emulateapj v. 14/09/00

A HIGH SPATIAL RESOLUTION ANALYSIS OF THE MAXIMA-1 COSMIC MICROWAVE BACKGROUND ANISOTROPY DATA

A. T. Lee[1,2,3], P. Ade[4], A. Balbi[2,3,5], J. Bock[6,7], J. Borrill[3,8], A. Boscaleri[9], P. de Bernardis[10], P. G. Ferreira[11,12], S. Hanany[3,13], V. V. Hristov[7], A. H. Jaffe[3], P. D. Mauskopf[14], C. B. Netterfield[15], E. Pascale[9], B. Rabii[1,2,3,16], P. L. Richards[1,3], G. F. Smoot[1,2,3,16], R. Stompor[3,16,17], C. D. Winant[1,3,16], J. H. P. Wu[18]

Draft version May 25, 2001

ABSTRACT

We extend the analysis of the MAXIMA-1 cosmic microwave background (CMB) data to smaller angular scales. MAXIMA, a bolometric balloon experiment, mapped a 124 deg^2 region of the sky with $10'$ resolution at frequencies of 150, 240 and 410 GHz during its first flight. The original analysis, which covered the multipole range $36 \leq \ell \leq 785$, is extended to $\ell = 1235$ using data from three 150 GHz photometers in the fully cross-linked central 60 deg^2 of the map. The main improvement over the original analysis is the use of $3'$ square pixels in the calculation of the map. The new analysis is consistent with the original for $\ell < 785$. For $\ell > 785$, where inflationary models predict a third acoustic peak, the new analysis shows power with an amplitude of 56 ± 7 μK at $\ell \simeq 850$ in excess to the average power of 42 ± 3 μK in the range $441 < \ell < 785$.

Subject headings: cosmic microwave background - cosmology: observations

1. INTRODUCTION

The power spectrum of temperature fluctuations in the cosmic microwave background (CMB) has recently been measured over a broad range of angular scales (de Bernardis et al. 2000; Hanany et al. 2000). The results are being used to discriminate between cosmological models and to determine cosmological parameters (Lange et al. 2000; Balbi et al. 2000; Dodelson & Knox 2000; Tegmark & Zaldarriaga 2000; Pierpaoli, Scott, & White 2000; Jaffe et al. 2000). There is strong evidence for a first peak in the power spectrum at $\ell \sim 200$ which is consistent with a flat universe in adiabatic inflationary models with cold dark matter. Fluctuations were also detected in the multipole range $400 \leq \ell \leq 785$ at smaller scales than those of the first peak.

MAXIMA is a balloon-borne experiment optimized to map the CMB anisotropy over a broad range of angular scales from $10'$ to $5°$. The first flight, MAXIMA-1, observed 124 square degrees of the sky. We have published an analysis of this data over the spherical harmonic multipole range $36 \leq \ell \leq 785$ (Hanany et al. 2000). In this paper, we extend the original analysis to $\ell = 1235$ using the data from three 150 GHz photometers. These measurements are a powerful discriminant between cosmological models and allow parameters to be determined with better accuracy. A companion paper Stompor et al. (2001) discusses the cosmological significance of these results.

The MAXIMA instrument is described in detail by Lee et al. (1999) and Hanany et al. (2000). In sections 2-4, we describe the analysis of the telescope beams, the pointing reconstruction, and the estimation of instrument noise, which are especially important for the high-ℓ region of the power spectrum. In section 5, we present the map and the angular power spectrum. In sections 6 and 7, we show that foreground contributions to the data are negligible and describe tests for systematic errors.

2. TELESCOPE BEAMS

[1] Dept. of Physics, University of California, Berkeley CA, USA
[2] Division of Physics,Lawrence Berkeley National Laboratory, Berkeley, CA, USA
[3] Center for Particle Astrophysics, University of California, Berkeley, CA, USA
[4] Queen Mary and Westfield College, London, UK
[5] Dipartimento di Fisica, Università Tor Vergata, Roma, Italy
[6] Jet Propulsion Laboratory, Pasadena, CA, USA
[7] California Institute of Technology, Pasadena, CA, USA
[8] National Energy Research Scientific Computing Center, Lawrence Berkeley National Laboratory, Berkeley, CA, USA
[9] IROE-CNR, Firenze, Italy
[10] Dipartimento di Fisica, Università La Sapienza, Roma, Italy
[11] Astrophysics, University of Oxford, Oxford, UK
[12] CENTRA, Instituto Superior Tecnico, Lisboa, Portugal
[13] School of Physics and Astronomy, University of Minnesota/Twin Cities, Minneapolis, MN, USA
[14] Department of Physics and Astronomy, University of Wales, Cardiff, UK
[15] Dept. of Physics and Astronomy, University of Toronto, Canada
[16] Space Sciences Laboratory, University of Californin, Berkeley, CA, USA
[17] Copernicus Astronomical Center, Warszawa, Poland
[18] Department of Astronomy, University of California, Berkeley, CA, USA

For a total-power radiometer such as MAXIMA, a finite telescope beam size introduces an exponential reduction in sensitivity at high-ℓ. Extending the MAXIMA power spectrum to higher ℓ values thus depends on an accurate knowledge of the beam patterns. Each of the 16 elements of the MAXIMA bolometer array were designed to have a FWHM Gaussian beam size of $10'$, which reduces power by a factor of five at $\ell \sim 1000$. The beams were measured in flight using observations of Jupiter, which has an angular diameter of $0.5'$. Observations were carried out at fixed elevation with the primary mirror scanning $\sim 4^\circ$ peak-peak in azimuth at 0.45 Hz and the gondola azimuth fixed. Sky rotation gave a raster map of Jupiter with more than 200 mirror scans across each array element. The reconstructed beam profiles have a peak signal-to-noise ratio of more than 1000. The beams are close to circular near the peak, but have a moderate asymmetry in the wings (see Fig. 9 in Wu et al. (2000)).

Wu et al. (2000) have developed a formalism for calculating the effects of asymmetric beams. We find that data measured with slightly asymmetric beams can be analyzed by using an effective symmetric beam. This formal treatment has been tested using simulated observations of a CMB sky with the observation strategy and measured beams for MAXIMA-1. Because of the high degree of symmetry near the beam centers, the estimated error in C_ℓ introduced by this technique is less than 1% at $\ell = 1000$.

The uncertainty in the measured beam profiles is a source of error at high ℓ. There is a 5% uncertainty in the measurement of the long and short axis FWHM, which is largely due to uncertainty in the baseline subtraction for each of the one-dimensional Jupiter scans. There are minor contributions to this error from uncertainties in pointing reconstruction and the measured bolometer time constant. This error gives an error in C_ℓ that increases with ℓ (Wu et al. 2000). The error is 6% at $\ell = 500$ and 17% at $\ell = 1000$. The errors in the ℓ bins are correlated, so the power spectrum will be biased either up or down with an amplitude that increases with ℓ.

3. POINTING RECONSTRUCTION

The MAXIMA experiment observes each sky pixel repeatedly to achieve an adequate signal-to-noise ratio. Errors in telescope pointing reconstruction smear the signal between pixels.

There are four temporal modulations of the beam in the MAXIMA experiment. The primary mirror scans in azimuth by $\sim 4^\circ$ peak-peak at ~ 0.45 Hz, the gondola scans in azimuth by $\sim 8^\circ$ peak-peak at ~ 20 mHz, sky rotation is used to scan in right ascension, and we map the same sky region twice during the flight at different elevations to achieve cross linking of pixels. Information from several sensors is combined to give the telescope pointing as a function of time, and each sensor contributes to the total pointing error.

The dominant pointing error comes from the primary mirror motion, as the mirror is rotated left or right. The elevation angle of the beams increases as the square of the azimuth scan angle. This elevation change can approach several arc minutes. We measure the centering of the primary mirror motion during flight with a $\sim 1^\circ$ uncertainty, which gives a $0.8'$ elevation uncertainty.

A CCD camera mounted to the inner frame of the gondola measures the attitude of the telescope by monitoring stars. A dedicated processor calculates the position of the two brightest stars in the field of the camera. By comparing the reconstructed and known separations of the stars, we estimate a $0.45'$ rms error in gondola orientation.

The total pointing reconstruction error is $0.95'$ rms, including the described contributions from the primary mirror position and the gondola attitude errors and several additional minor contributions. Although some of the pointing errors are systematic rather than random, the multiple modulations in MAXIMA's observation strategy tend to randomize the errors when projected on the sky. Therefore, we model the pointing error as a simple Gaussian distributed error.

We simulate an observation with such a Gaussian pointing reconstruction error to assess the effect on the measured power spectrum. As expected, the main effect is a systematic underestimate of power at high ℓ. In principle, this bias is predictable and can be accounted for accurately. However, since the pointing error is not perfectly Gaussian, we conservatively assign a symmetric random error equal to the size of the bias which is $\delta C_\ell / C_\ell \sim 10\%$ at $\ell = 1000$. The C_ℓ error for each ℓ bin due to pointing reconstruction error is given in Table 1. As with the beam shape uncertainty, this fully correlated error has the effect of increasing or decreasing power monotonically with increasing ℓ.

4. NOISE ESTIMATION

The data contain both the signal from the sky and noise from the detector system. The procedures for map making and power spectrum estimation require an accurate estimate of the detector system noise to correctly estimate the signal. The accuracy of the noise estimation is most critical in the high-ℓ portion of the power spectrum, where the data become increasingly noise dominated. This trend occurs because C_ℓ falls roughly as ℓ^2 and because the telescope beam reduces the signal at high ℓ.

As described in (Hanany et al. 2000), we observe a spurious primary-mirror synchronous signal which complicates the noise estimation because it is larger than the rms amplitude of the noise. We use two methods to estimate the detector noise. In the first method, we assume that noise dominates the signal at all frequencies other than the primary mirror modulation frequency and its harmonics. The noise at those frequencies is calculated by interpolating data from the power spectrum at nearby frequencies. In the second method, we use the iterative noise estimation procedure of Ferreira & Jaffe (2000). Here, the noise and signal are both estimated iteratively in the map-making stage. We iterate the noise using a map with $8'$ pixels to limit computation time. This resolution should be sufficient, since the signal power decreases at smaller angular scales.

We make $3'$-resolution maps using the two noise estimates. We calculate the power spectrum for $\sim 23,000$ pixels in the "central" region of the maps, and we find that the difference between the two spectra is much less than the statistical error for all ℓ bins. This central region covers roughly half the area of the map (60 deg^2) where the observations are fully cross linked, the sampling is the most uniform, and the signal-to-noise ratio is highest. In this way, we reduce both the time required to search for systematic errors and the computation time. This procedure increases statistical error bars by $< 10\%$ for $\ell > 500$ and by $< 3\%$ at $\ell = 1000$.

The power spectrum of the difference between maps from two photometers in the array is a stringent test of the noise estimation process. A mis-estimate of the white noise level of the detector system gives a power spectrum that diverges from zero as ℓ^2. Correlation in the noise between detectors can give the same behavior. In a separate analysis we do not find significant correlation between the time streams in the 0.1 - 30 Hz frequency range used in the analysis aside from that caused by the spurious chopper-synchronous signal. This signal is removed during the map making stage resulting in maps without correlations. We also find that histograms of the temperatures in the $8'$ difference maps are consistent with the distributions expected for no noise correlations at a Kolmogorov-Smirnov significance level larger than 10%. As discussed in section 7, the power spectra obtained using difference maps are consistent with zero, with no apparent systematic divergence at high ℓ.

5. MAP AND ANGULAR POWER SPECTRUM

The map-making and power spectrum analysis procedures are similar to those described by Hanany et al. (2000). In that analysis we used $5' \times 5'$ pixels to limit computation time, and we limited the analysis to an ℓ range where such pixelization does not bias the results. In principle, the smearing effect of larger pixels can be accounted for by deconvolving a pixel window function. In practice, however, this procedure may introduce a systematic bias in the power spectrum due to the uneven spatial distribution of samples in each pixel. We choose a $3'$ square pixel for the present analysis, since this pixel size does not compromise the resolution of the map (Wu et al. 2000).

In this paper, we report on the analysis of data from three 150 GHz photometers using a $3'$ pixelized map. Hanany et al. (2000) analyzed the data from three 150 GHz photometers and a 240 GHz photometer using $5'$ pixelization. The data from all four photometers passed all tests for consistency up to $\ell = 785$. In this work with $3'$ pixels, we exclude the 240 GHz data because it does not pass consistency tests above $\ell = 785$. The power spectrum of difference maps between the 240 GHz data and any 150 GHz data are inconsistent with zero in this high ℓ region. One possible reason for this discrepancy is that the spurious primary-mirror synchronous signal is larger by a factor > 2 in the 240 GHz data compared to the 150 GHz data.

The raw data preparation is described in Hanany et al. (2000). We remove data during calibration events, and we also remove short sections of data which deviate by $> 4\ \sigma$ such as cosmic ray events and telemetry drop-outs. We deconvolve the transfer functions of the bolometers and readout electronics and estimate the noise power spectrum from sections of the time stream that had no long gaps (Stompor et al., in preparation). We marginalize over frequencies lower than 0.1 Hz and higher than 30 Hz, where we do not expect appreciable optical signals.

The data are calibrated using observations of the CMB dipole, and periodic optical stimulator events are used to account for a small drift in calibration during the flight (Hanany et al. 2000). The calibrated time stream data, the pointing solution, and the estimate of the noise power spectrum are combined to produce a maximum likelihood pixelized map of temperature anisotropy and a pixel-pixel noise correlation matrix for each photometer (Wright 1996; Tegmark 1997; Bond et al. 1999) using the MADCAP software package (Borrill 1999).

A combined maximum-likelihood temperature anisotropy map is produced by adding individual maps with a weight inversely proportional to their noise correlation matrices. This map, shown in Figure 1, contains $\sim 40,000$ $3'$ square pixels. We assign a calibration uncertainty of 4% to the magnitude of temperature fluctuations in the combined map (Hanany et al. 2000).

We calculate the angular power spectrum C_ℓ of the central region of the combined map using the MADCAP (Borrill 1999) implementation of the maximization of the likelihood function following Bond, Jaffe & Knox (1998). The MADCAP implementation assumes that the beam shape has axial symmetry. We produce an effective beam for the analysis of the combined map by noise-weighted averaging the individual beams. As discussed in section 2, we follow the procedure of Wu et al. (2000) to find a symmetric approximation for the effective beam. We apply no corrections for the negligible ($< 1\%$ at $\ell = 1000$) smoothing of the $3'$ pixels.

We calculate the power spectrum of the temperature fluctuations using 15 bins in ℓ over the range $3 \lesssim \ell \lesssim 1800$ assuming a constant $\ell(\ell+1)C_\ell$ band power in each bin, and marginalizing over the CMB monopole and dipole.

The benefits of only using the central region of the map for power spectrum analysis are discussed in section 4. The penalty is an increased error that falls with increasing ℓ due to the rise in sample variance. To minimize this effect, we create a composite power spectrum which uses the $\ell < 335$ points from the original Hanany et al. (2000) analysis. We choose this transition point to limit the maximum error bar increase to $\sim 20\%$. For bins with $\ell < 335$, we marginalize over all the higher ℓ bins from Hanany et al. (2000). For the bins with $\ell > 335$ obtained using the central region, we marginalize over the bins at $\ell < 335$ and $\ell > 1235$. For both ℓ regions, we diagonalize the ℓ-bin correlation matrix using a variant of techniques discussed in Bond, Jaffe & Knox (1998). The correlations between the dominant bin and adjacent bins are typically less than 10%.

Table 1 lists the dominant bins, the C_ℓ estimates, and the $\Delta T = \sqrt{\ell(\ell+1)C_\ell/2\pi}$ estimates for the corresponding uncorrelated linear combinations of bins. We quote 1σ errors on the C_ℓ estimates assuming 68% confidence intervals using the offset log-normal distribution model of Bond, Jaffe & Knox (2000). These statistical errors do not include three additional independent sources of systematic uncertainty, which are fully correlated between ℓ bins. The 1σ calibration error is a constant 8% of $\ell(\ell+1)C_\ell/2\pi$. The ℓ-dependent errors due to the beam-diameter uncertainty and pointing reconstruction uncertainty are given in Table 1. Information on the shape of the bin-power likelihood functions and window functions will be made available on the MAXIMA web site

ℓ_{eff}	$[\ell_{min}, \ell_{max}]$	$\ell(\ell+1)C_\ell/2\pi$ (μK^2)	Beam Error (%)	Pointing Error (%)	ΔT (μK)
77	[36, 110]	1999^{+675}_{-506}	± 0	± 0	45^{+7}_{-6}
147	[111, 185]	2960^{+682}_{-554}	± 0.6	± 0.2	54^{+6}_{-5}
222	[186, 260]	6092^{+1052}_{-901}	± 1.5	± 0.4	78^{+6}_{-6}
294	[261, 335]	3830^{+670}_{-577}	± 2.5	± 0.8	62^{+5}_{-5}
381	[336, 410]	2270^{+569}_{-471}	± 3.5	± 1.2	48^{+6}_{-5}
449	[411, 485]	1468^{+387}_{-325}	$^{+5}_{-4.5}$	± 1.7	38^{+5}_{-4}
523	[486, 560]	1935^{+475}_{-408}	$^{+6.5}_{-6}$	± 2.3	44^{+5}_{-5}
597	[561, 635]	1811^{+511}_{-441}	$^{+8}_{-7}$	± 3.0	43^{+6}_{-6}
671	[636, 710]	2100^{+629}_{-546}	$^{+9.5}_{-8.5}$	± 3.7	46^{+6}_{-6}
746	[711, 785]	2189^{+777}_{-680}	$^{+11}_{-10}$	± 4.6	47^{+8}_{-8}
856	[786, 935]	3104^{+805}_{-738}	$^{+14}_{-12}$	± 5.6	56^{+7}_{-7}
1004	[936, 1085]	1084^{+1219}_{-1085}	$^{+18}_{-15}$	± 7.7	33^{+13}_{-22}
1147	[1086, 1235]	223^{+2791}_{-2025}	$^{+25}_{-18}$	± 10.2	15^{+29}_{-15}

Table 1

Uncorrelated Power Spectrum from the MAXIMA-1 map. Data for $\ell < 335$ are from the power spectrum of the full map with $5'$ pixels, and data for $\ell > 335$ are from the power spectrum of the central region of the map with $3'$ pixels. Errors are the 68% integrated probability of the offset log-normal likelihood functions with a constant prior in either $\ell(\ell+1)C_\ell/2\pi$ or $\Delta T = \sqrt{\ell(\ell+1)C_\ell/2\pi}$ for their respective columns. Here $[\ell_{min}, \ell_{max}]$ gives the ranges of the dominant bins. The correlated beam errors are described in the text.

(http://cfpa.berkeley.edu/maxima).

The top panel of Figure 2 shows the maximum likelihood power spectrum and an inflationary adiabatic model that best fits the Hanany et al. (2000) MAXIMA-1 and COBE/DMR power spectra. The results for $\ell < 785$ are consistent with those in Hanany et al. (2000). The model has $(\Omega_b, \Omega_{cdm}, \Omega_\Lambda, n, h) = (0.07, 0.61, 0.23, 1, 0.60)$ (Balbi et al. 2000). The χ^2 for this model is 37 for all 41 data points. If we only use the 13 data points of MAXIMA-1 we obtain $\chi^2 = 5$ for this model. In both cases, we are fitting with an 7 parameter inflationary model.

6. FOREGROUNDS

Foreground sources include: emission from the earth, the atmosphere, and galactic dust, free-free and synchrotron radiation, point sources, and scattering due to the Sunyaev-Zel'dovich effect. The analysis of Hanany et al. (2000) for $\ell < 785$ is applicable for sources that are expected to be less strong at small angular scales. In that work, we argue that the detected signal is inconsistent with an atmospheric or ground-based origin due to its temporal stability. We can detect dust contamination in our maps, but at a negligible level of 2.3 μK at 150 GHz. Estimates of bremsstrahlung and synchrotron radiation (Bouchet & Gispert 1999) predict contributions of less than 1 μK at 150 and 240 GHz. The ratio of detected power between 150 and 240 GHz is consistent with the CMB and inconsistent with dust, synchrotron, and free-free emission.

Point sources are the foreground of concern for the high-ℓ region data presented in this paper. A catalog search (Sokasian, Gawiser, & Smoot 2000; Gawiser & Smoot 1997) yielded no detectable radio or infra-red sources in any of the frequency bands. The "pessimistic" model of Tegmark et al. (2000) predicts ~ 20 μK rms point source contamination at $\ell = 1000$, which is small compared to our statistical errors. The shape of the power spectrum is inconsistent with a point source origin, which would give a rising spectrum with increasing ℓ. Instead, the power spectrum decreases above $\ell = 850$ and is consistent with zero. A broad bin covering $1235 < \ell < 1800$ (not tabulated) is consistent with zero at the 1 σ level.

7. TESTS FOR SYSTEMATIC ERRORS

In the original data analysis of Hanany et al. (2000), we found no evidence for uncorrected systematic errors over the range $35 < \ell < 785$ after performing a suite of tests. Although maps with $8'$ and $10'$ resolution give power spectra with a systematic bias at high ℓ, they are still useful for systematic error tests especially in the case where the result is a null power spectrum. We confirm that the following combinations of data produce a spectrum with no signal over the range $35 < \ell < 1235$: (1) a dark bolometer, (2) the data from the 410 GHz photometer, (3) the difference between the overlapping part of the combined map from the CMB-1 and -2 scans, and (4) the differences between the maps produced by different photometers. We repeated the fourth test on the central region of the map using $3'$ pixels. We calculated the difference of one and the sum of the other two as shown in Fig. 2

8. DISCUSSION

We have presented a measurement of the angular power spectrum of the CMB over a range of angular scales corresponding to the multipole range $36 < \ell < 1235$, which is the largest yet reported by a single experiment. The data for $\ell > 400$ can be fit to a flat line of amplitude 1860 μK^2 with a $\chi^2 \sim 5$ for 7 d.o.f. However, if we focus on the bin at $\ell \sim 850$, we find that its amplitude of 56 ± 7 μK is in excess to the average power of 42 ± 3 μK in the range $441 < \ell < 785$ at a confidence level of $\sim 95\%$. This confidence level calculation is presented in the companion paper by Stompor et al. (2001). This excess power is consistent with the third acoustic peak predicted in this region by inflationary adiabatic models. The power spectrum is well fit by such a model over the entire range of ℓ.

We thank Danny Ball and the other staff at NASA's National Scientific Balloon Facility in Palestine, TX for their outstanding support of the MAXIMA program. MAXIMA is supported by NASA Grants NAG5-3941, NAG5-6552, NAG5-4454, GSRP-031, and GSRP-032, and by the NSF through the Center for Particle Astrophysics at UC Berkeley, NSF cooperative agreement AST-9120005, and KDI grant 9872979. The data analysis used resources of the National Energy Research Scientific Computing center which is supported by the Office of Science of the U.S. Department of Energy under contract no. DE-AC03-76SF00098, and the resources of the Minnesota Supercomputing Institute. PA acknowledges support from PPARC rolling grant, UK.

REFERENCES

Balbi, A., *et al.* 2000, ApJ, 545, L1, astro-ph/0005124
Bond, J. R., Crittenden, R., Jaffe, A. H., & Knox, L. E. 1999, Computing in Science and Engineering, 1, 21, astro-ph/9903166.
Bond, J. R., Jaffe, A. H., & Knox, L. 1998, Phys. Rev. D, 57, 2117, astro-ph/9708203
Bond, J. R., Jaffe, A. H., & Knox, L. 2000, ApJ, 533, 19 astro-ph/9808264
Borrill, J. 1999, in EC-TMR Conference Procedings 476, 3K Cosmology, ed. L. Maiani, F. Melchiorri, & N. Vittorio (Woodbury, New York: AIP), 277
Bouchet, F., & Gispert, R. 1999, New Astronomy, 4, 443
de Bernardis, P., et al. 2000, Nature, 404, 955
Dodelson, S., & Knox, L. 2000, Phys. Rev. Let, 84, 3523
Ferreira, P. G., & Jaffe, A. H. 2000, MNRAS, 312, 89, astro-ph/9909250
Gawiser, E., & Smoot G. 1997, ApJ, 480, L1, astro-ph/9603121
Hanany, S., *et al.* 2000, ApJ, 545, L5, astro-ph/0005123
Jaffe, A. H., *et al.* 2001, Phys. Rev. Let, 86, 3475, astro-ph/0007333
Lange, A. E., *et al.* 2001, Phys. Rev D., 63, 042001, astro-ph/0005004
Lee, A. T., *et al.* 1999, in EC-TMR Conference Procedings 476, 3K Cosmology, ed. L. Maiani, F. Melchiorri, & N. Vittorio (Woodbury, New York: AIP), 224, astro-ph/9903249
Pierpaoli, E., Scott, D., & White, M. 2000, Science, 287, 2171
Sokasian, A., Gawiser, E. & Smoot G. 2000, ApJ, submitted, astro-ph/9811311
Stompor, R., *et al.* 2001, in preparation
Tegmark, M. 1997, ApJ, 480, L87
Tegmark, M., Eisenstein, D., Hu, W., & De Oliveira-Costa, A. 2000, ApJ, 530, 133, astro-ph/9905257
Tegmark, M., & Zaldarriaga, M., 2000, ApJ, 544, 30, astro-ph/0002091
Wright, E. L. 1996, presented at the IAS CMB Data Analysis workshop, astro-ph/9612006
Wu, J. H. P., *et al.* 2001, ApJS, 132, 1, astro-ph/0007212

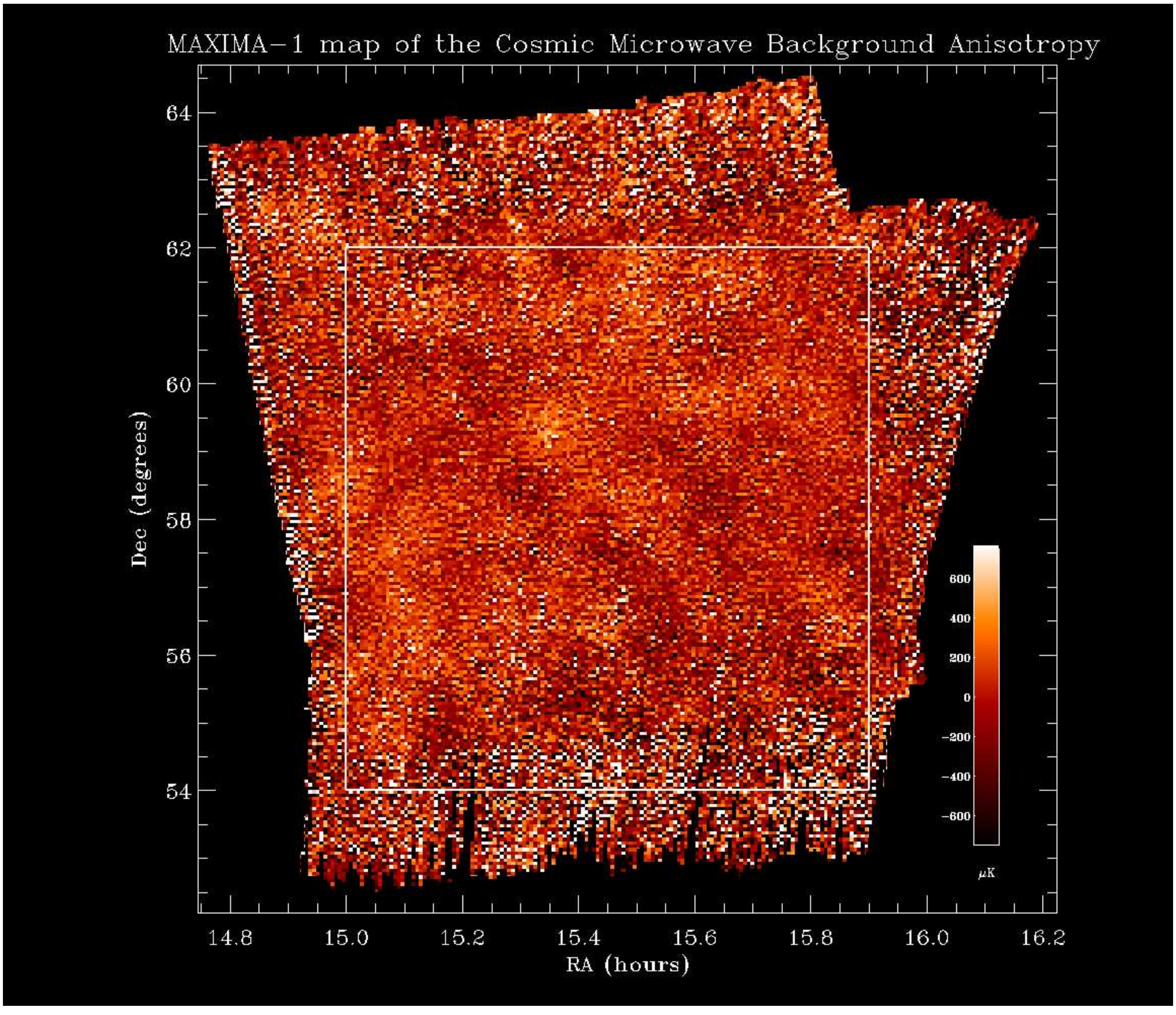

FIG. 1.— A maximum-likelihood map of the CMB anisotropy from MAXIMA-1. The resolution is determined by the 10′ FWHM Gaussian beam of the telescope. The map is made using data from three 150 GHz photometers and contains $\sim 40,000$ $3' \times 3'$ pixels. We use the central region of the map (outlined) to compute the power spectrum presented in Fig. 2. This region is fully cross linked, has the most uniform sampling, and has the highest signal-to-noise ratio. The area of the central region is 60 deg^2 and contains $\sim 23,000$ pixels.

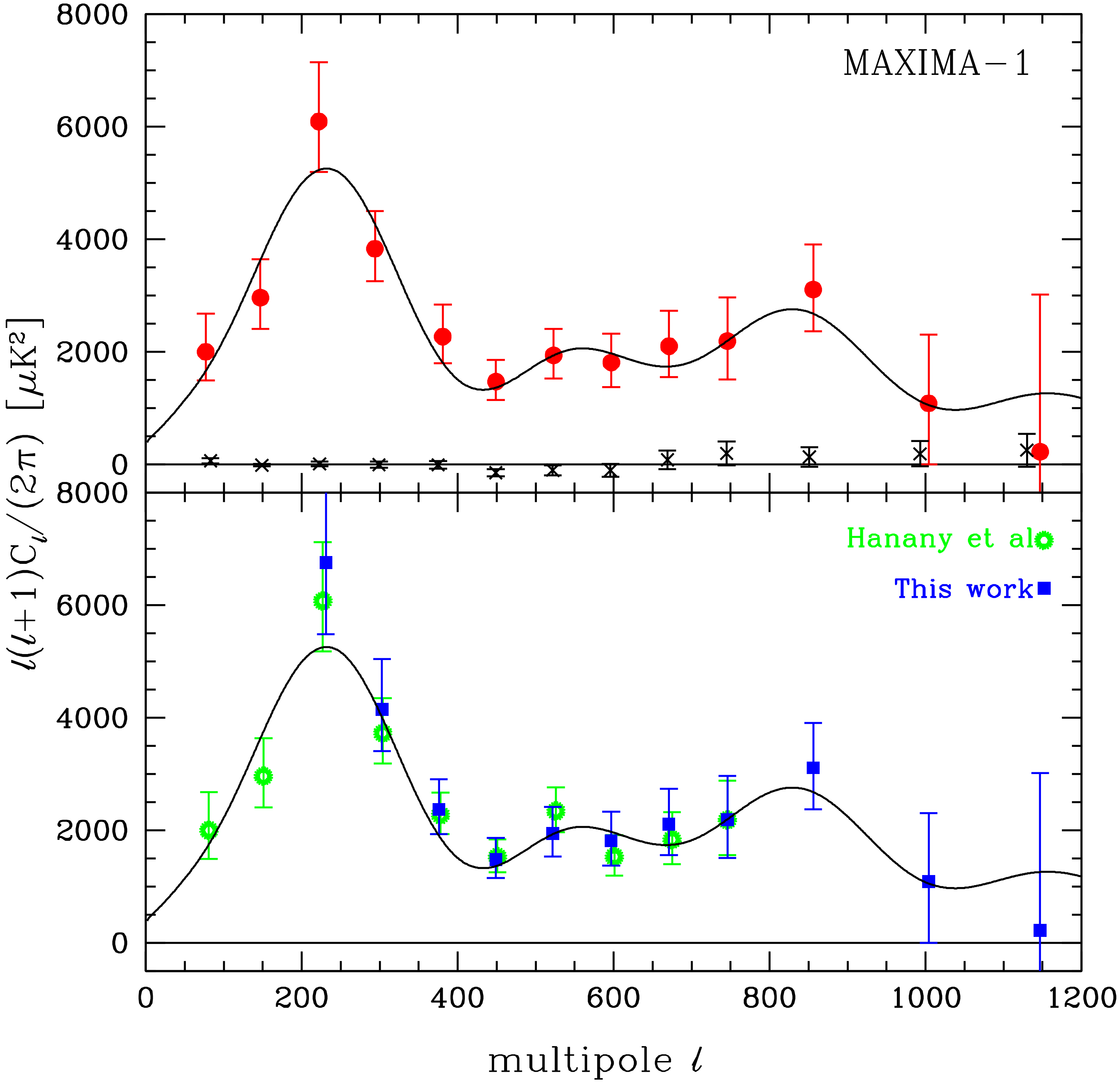

FIG. 2.— Top panel: Composite angular power spectrum of the CMB anisotropy from the MAXIMA-1 map (filled circles). The points for $\ell < 335$ are from the power spectrum of the full $5'$ pixelized map from Hanany et al. (2000), and the points for $\ell > 335$ are from the power spectrum of the central region of the $3'$ pixelized map shown in Fig. 1. The error bars are 68% confidence intervals calculated using the offset log-normal likelihood functions of Bond, Jaffe & Knox (2000). The solid curve is the best fit (ΛCDM) inflationary adiabatic cosmology to the MAXIMA-1 and COBE/DMR data. The model has $(\Omega_b, \Omega_{cdm}, \Omega_\Lambda, n, h) = (0.1, 0.6, 0.3, 1.08, 0.53)$ (Balbi et al. 2000). The crosses are the estimated power spectrum of the difference between two independent maps, the first given by one of the three photometers and the other from the sum of the other two. Bottom panel: A comparison between the Hanany et al. (2000) power spectrum and the power spectrum of the central region of the $3'$ pixelized map shown in Fig. 1. For the $3'$ central region data, the power spectrum for $\ell < 186$ is not well constrained.